Dynamics of a non-Hermitian Floquet Wannier-Stark system

H. P. Zhang, K. L. Zhang and Z. Song*

School of Physics, Nankai University, Tianjin 300071, China

* songtc@nankai.edu.cn

Abstract

We study the dynamics of the non-Hermitian Floquet Wannier-Stark system in the framework of the tight-binding approximation, where the hopping strength is a periodic function of time with Floquet frequency ω. It is shown that the energy level of the instantaneous Hamiltonian is still equally spaced and independent of time t and the Hermiticity of the hopping term. In the case of off resonance, the dynamics are still periodic, while the occupied energy levels spread out at the resonance, exhibiting t^z behavior. Analytical analysis and numerical simulation show that the level-spreading dynamics for real and complex hopping strengths exhibit distinct behaviors and are well described by the dynamical exponents $z = 1$ and $z = 1/2$, respectively.

Received Date
Accepted Date
Published Date

Contents

1 Introduction

The Hermitian and static system is the main study object of traditional quantum mechanics, preserving the reality and conservation of energy. When these two constraints are violated, the properties of the material could be drastically modified, leading to new phases and phenomena [1, 2] without analogs in their static or Hermitian counterparts. Floquet engineering has facilitated the exploration of diverse dynamic, topological, and transport phenomena across a wide range of physical contexts. More recently, the Floquet approach has been employed to engineer topological phases in non-Hermitian systems. Importantly, it was discovered that the interplay between time-periodic driving fields and the presence of gain, loss, or nonreciprocal effects can lead to the emergence of topological phases exclusive to non-Hermitian Floquet systems [3–12] .

Motivated by the above investigations, the aim of the present paper is to examine how non-Hermiticity and periodic driving impact a Stark ladder system. Specifically, we study the dynamics of the non-Hermitian Floquet Wannier-Stark system in the framework of the tight-binding approximation. A conventional Wannier-Stark ladder consists of quantized equidistant energy levels, which separated by the Bloch frequency and emerge in a periodic Hermitian system under a linear potential [13]. Recent works [14–17] show that non-Hermitian hopping terms, including asymmtric and complex strengths, remain the reality of the Wannier-Stark ladder. On the other hand, it has proposed that a time-dependent hopping strength for a Bloch system can be realized by dynamically modulated waveguide arrays [18].

In this work, we introduce non-Hermiticity and periodic driving by focusing on cosinusoidal time-dependent hopping strength with frequency ω and complex amplitude. The main reason for choosing such systems is that the energy level of the instantaneous Hamiltonian is still equally spaced with ω_0 and independent of time t and the Hermiticity of the hopping strength. This allows us to investigate the dynamics based on analytical solutions. We find that, in the case of off resonance, the dynamics are still periodic, while the occupied energy levels spread out at the resonance, exhibiting t^z behavior. Analytical analysis and numerical simulation show that the level-spreading dynamics for real and complex hopping strengths exhibit distinct behaviors and are well described by the dynamical exponents $z = 1$ and $z = 1/2$, corresponding to superdiffusion and diffusion, respectively [19–21]. These findings may help us deepen our understanding of the interplay between non-Hermiticity and periodic driving impacts on the dynamics of the system. In addition, we propose a scheme to demonstrate the results by wavepacket dynamics in a 2 D square lattice.

This paper is organized as follows. In Sec. 2, we introduce a non-Hermitian time-dependent tight-binding model supporting a Wannier-Stark ladder and present the analytical eigenstates of the instantaneous Hamiltonian. In Sec. 3, we focus on the dynamics of the static system, while the Floquet system at resonance in Sec. 4. Sec. 5 describes the application of the solutions to a specific initial state. In Sec. 6, a scheme for the simulator of our results is proposed in the framework of wavepacket dynamics in a 2D square lattice. Finally, we summarize our results in Sec. 7.

2 Model and generalized Wannier-Stark ladder

We start with the tight-binding model with the Hamiltonian

$$H = \kappa(t) \sum_{n=-\infty}^{+\infty} (|n\rangle\langle n+1| + \text{ H.c}) + \omega_0 \sum_{n=-\infty}^{+\infty} n|n\rangle\langle n|, \tag{1}$$

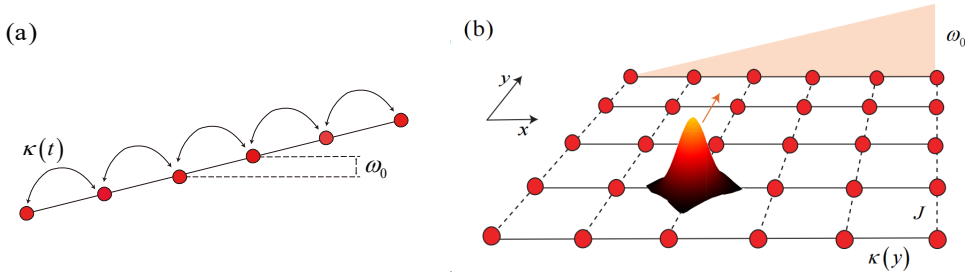

Figure 1: (a) Schematic illustrations of the Hamiltonian in Eq. (1), which represents a tight-binding chain with a time dependence on the hopping strength between two adjacent sites. The on-site potential is tilted with slope ω_0. It is shown that such a system supports a Stark-ladder with time-independent energy-level spacing. (b) Schematic illustrations of the Hamiltonian in Eq. (44), which is a tight-binding model of a square lattice with time-independent system parameters. The contributions of hopping strength and on-site potential can be used to simulate the dynamics of system (a).

where $|n\rangle$ denotes a site state describing the Wannier state localized on the nth period of the potential. Here, $\kappa(t)$ is the time-dependent tunneling strength, while ω_0 is the slope of the linear potential from a static force. Fig. 1(a) shows a schematic of the system. In our study, κ can be real and complex. It is well known that the spectrum of H is equally spaced when κ is a real constant, supporting periodic dynamics [22–24]. This phenomenon has been observed in systems of semiconductor superlattices and ultracold atoms [25–28].

Now, we extend the conclusion to the case with arbitrary κ. The eigenstate of $|\psi_m\rangle$ can always be written in the form

$$|\psi_m\rangle = \sum_n c_{nm}|n\rangle, \tag{2}$$

satisfying the Schrödinger equation

$$H|\psi_m\rangle = E_m|\psi_m\rangle. \tag{3}$$

The coefficient c_{nm} is determined by the equation

$$c_{n+1,m} + c_{n-1,m} = \frac{E_m - n\omega_0}{\kappa} c_{nm}, \tag{4}$$

which accords with the recurrence relation of the Bessel function J_n of argument x, i.e.,

$$J_{n+1}(x) + J_{n-1}(x) = 2\frac{n}{x}J_n(x). \tag{5}$$

Then, we have

$$c_{nm} = J_{n-m}(-\frac{2\kappa}{\omega_0}), E_m = m\omega_0. \tag{6}$$

We can see that the eigenenergy $m\omega_0$ is independent of κ, regardless of whether it is real or complex. This is crucial for the main conclusion of this work. Although the profile of the eigenstate

$$\psi_m(n) = \langle n|\psi_m\rangle = J_{n-m}(-\frac{2\kappa}{\omega_0}), \tag{7}$$

in real space is κ dependent, and it is always localized. The inverse participation ratio (IPR) is a simple way to quantify the localization of a given state. For spatially extended states, the

value of the IPR approaches zero when the system is sufficiently large, whereas it is finite for localized states regardless of the system size. The IPR of the eigenstate $|\psi_m\rangle$ is

$$\mathrm{IPR}_m = \frac{\sum_n |\langle n|\psi_m\rangle|^4}{(\sum_n |\langle n|\psi_m\rangle|^2)^2} = \frac{\sum_n |J_{n-m}(-\frac{2\kappa}{\omega_0})|^4}{(\sum_n |J_{n-m}(-\frac{2\kappa}{\omega_0})|^2)^2}. \tag{8}$$

Numerical simulations show that IPR_m is independent of m and N for a sufficiently large N. We have $\mathrm{IPR}_m = 0.418$ and 0.534 for $-2\kappa/\omega_0 = 1.0$ and $1.0i$, respectively, which indicates that $|\psi_m\rangle$ is in a localized state. In parallel, without loss of generality, we have

$$|\varphi_m\rangle = \sum_n J_{n-m}(-\frac{2\kappa^*}{\omega_0})|n\rangle, \tag{9}$$

for the equation

$$H^\dagger |\varphi_m\rangle = m\omega_0 |\varphi_m\rangle, \tag{10}$$

which establishes the biorthonormal set $\{|\varphi_m\rangle, |\psi_n\rangle\}$, satisfying

$$\langle\varphi_m|\psi_n\rangle = \sum_{n'} J^*_{n'-m}(-\frac{2\kappa^*}{\omega_0})J_{n'-n}(-\frac{2\kappa}{\omega_0}) = \delta_{mn}, \tag{11}$$

since the eigenlevels are independent of κ, without coalescence of eigenvectors. This is an important basis for the following investigations.

3 Bloch oscillation in a non-Hermitian system

Now, we consider the dynamics of the system with slowly varying $\kappa(t)$. When κ is time independent, the dynamics of the system are governed by the propagator

$$U_{mn}(t) = \langle m|e^{-iHt}|n\rangle. \tag{12}$$

Employing the biorthonormal set $\{|\varphi_m\rangle, |\psi_n\rangle\}$, we have

$$\begin{aligned} U_{mn}(t) &= \sum_l \langle m|\psi_l\rangle e^{-iE_l t}\langle\varphi_l|n\rangle \\ &= J_{m-n}(-\frac{4\kappa}{\omega_0}\sin\frac{\omega_0 t}{2})e^{-i(m-n)\frac{\omega_0 t}{2}} i^{m-n} e^{-in\omega_0 t}, \\ &= i^{m-n} e^{-i(m+n)\frac{\omega_0 t}{2}} J_{m-n}(-\frac{4\kappa}{\omega_0}\sin\frac{\omega_0 t}{2}), \end{aligned} \tag{13}$$

which is a periodic function with period $2\pi/\omega_0$. For a given initial state

$$|\Phi(0)\rangle = \sum_l c_l |l\rangle \tag{14}$$

the Dirac probability distribution in real space for the evolved state $|\Phi(t)\rangle$ is

$$P_m(t) = |\langle m|\Phi(t)\rangle|^2 = \left|\sum_l c_l U_{ml}(t)\right|^2, \tag{15}$$

which is still periodic. We obtain the conclusion that the total Dirac probability

$$P(t) = \sum_n P_n(t), \tag{16}$$

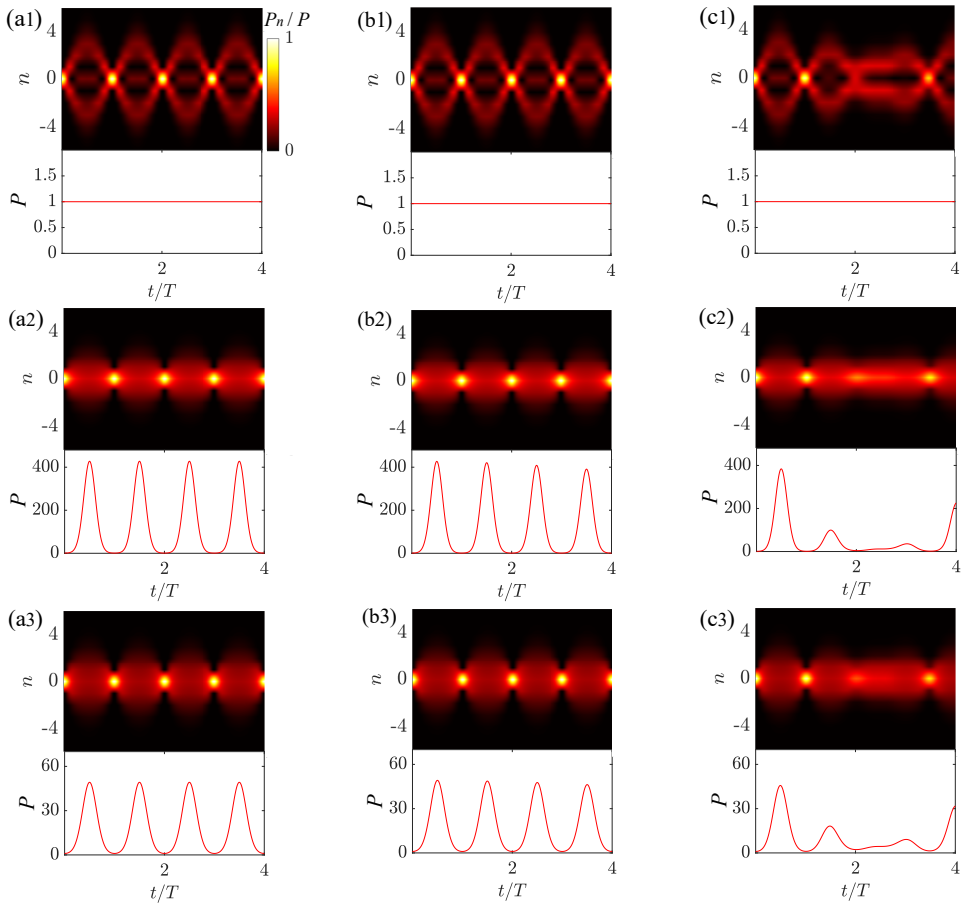

Figure 2: Plots of $P_n(t)/P(t)$ (see the main text) and $P(t)$ defined in Eqs. (15) and (16), obtained by numerical diagonalization for several typical values of system parameters with $\omega_0 = 1$. Here, (a1), (b1), and (c1) correspond to the cases with $\omega = 0$, 0.01, and 0.1, respectively, and $\kappa_0 = 1$. (a2), (b2), and (c2) correspond to the cases with $\omega = 0$, 0.01 , and 0.1, respectively, and $\kappa_0 = i$. (a3), (b3),and (c3) correspond to the cases with $\omega = 0$, 0.01, and 0.1, respectively, and $\kappa_0 = e^{i\pi/4}$. We can see that the patterns in (a2)(b2)(c2) and (a3)(b3)(c3) are similar. This inidcates that the imaginary part of hopping plays an important role in the shapes of evolved states.

is still periodic, regardless of whether κ is real or complex.

In this work, we explore what happens when κ is time dependent. According to the adiabatic theorem, the expression of $U_{mn}(t)$ still holds true for slowly varying $\kappa(t)$ during a short period of time. Considering the case with $\kappa(t) = \kappa_0 \cos(\omega t)$, where κ_0 can be a complex number and the frequency of κ is small, $\omega \ll \omega_0$. It can be predicted that $|\Phi(t)\rangle$ and $P(t)$ are still approximately periodic even for the quasiadiabatic process. However, this approach could be invalid for the diabatic process.

To verify and demonstrate the above analysis, numerical simulations are performed to investigate the dynamic behavior of dynamic processes with different values of ω/ω_0. We compute the temporal evolution of a site state, $|\Phi(0)\rangle = |0\rangle$ by using a uniform mesh in the time discretization for the time-dependent Hamiltonian $H(t)$. The evolved state is

$$|\Phi(t)\rangle = \mathcal{T} \exp\left[-i \int_0^t H(t)\,\mathrm{d}t\right] |\Phi(0)\rangle\,, \tag{17}$$

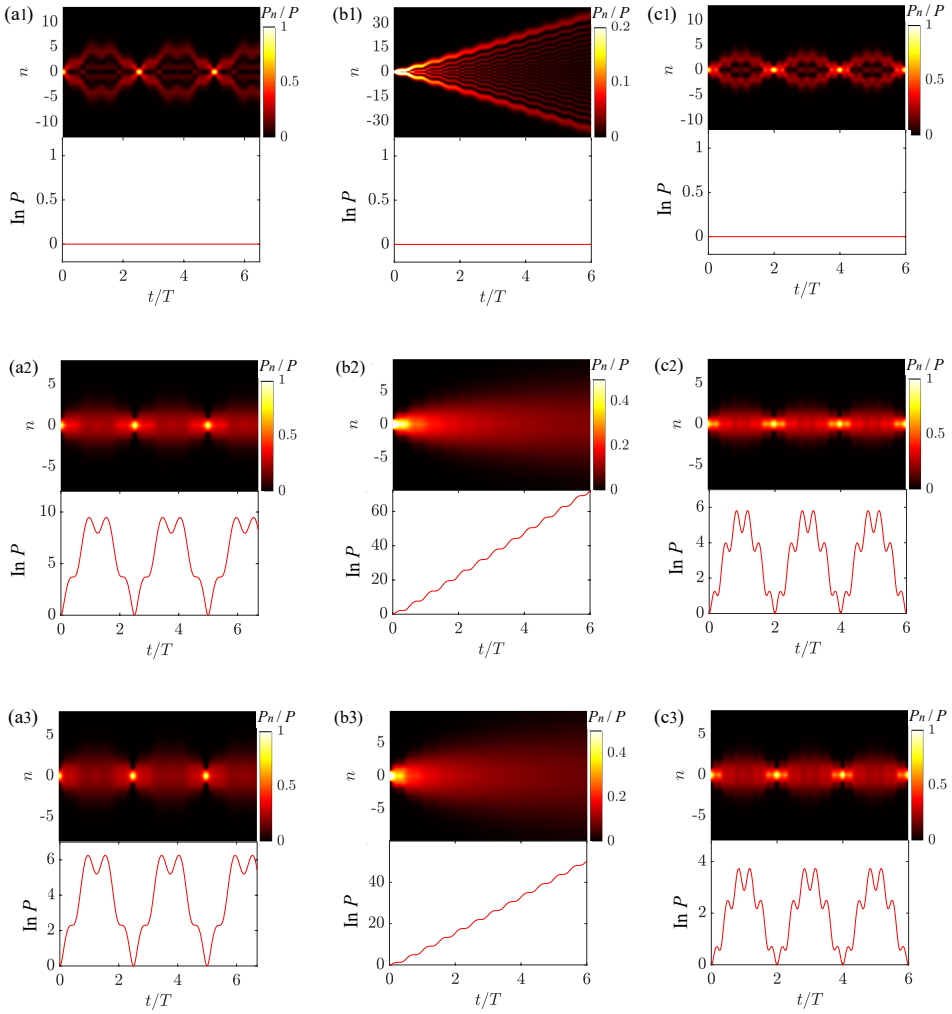

Figure 3: Plots of $P_n(t)/P(t)$ (see the main text) and In$P(t)$ defined in Eqs. (15) and (16), obtained by numerical diagonalization for several typical values of system parameters with $\omega_0 = 1$. Here, (a1), (b1), and (c1) correspond to the cases with $\omega = 0.6$, 1, and 1.5, respectively, and $\kappa_0 = 1$. (a2), (b2), and (c2) correspond to the cases with $\omega = 0.6$, 1 , and 1.5, respectively, and $\kappa_0 = i$. (a3), (b3),and (c3) correspond to the cases with $\omega = 0.6$, 1, and 1.5, respectively, and $\kappa_0 = e^{i\pi/4}$.

where $\mathcal{T}$ is the time-order operator. Figs. 2 and 3 are the plots of $P_n(t)/P(t)$ and $P(t)$ for several typical values of ω/ω_0. For the non-Hermitian systems, the difference between the maximum and minimum of $P(t)$ is very large. Thus the profile of the evolved state cannot be properly presented by the plot of $P_n(t)$. To present a complete and visible profile, we plot the rescaled P_n by $P_n(t)/P(t)$. When the total probability $P(t)$ is periodic in time, the periodicity of the evolved state can be confirmed by the profile of the probability distribution.

The numerical results indicate that the Bloch oscillation exists for small ω/ω_0. For non-Hermitian cases, the profile of the evolved state does not change substantially, but the probability is periodic or quasiperiodic. From Fig. 3 we can see that the evolution of the profile of the evolved state is still periodic when $\omega \neq \omega_0$, but is not periodic at $\omega = \omega_0$. Ihis indicates that the dynamics are peculiar at resonance, which is the focus of the paper.

4 Floquet-resonance dynamics

Now, we investigate the dynamics of the system with time-dependent $\kappa(t)$. When $\kappa(t)$ is periodic, the system becomes a Floquet system. The solution of the Schrödinger equation

$$i\frac{\partial}{\partial t}|\Psi(t)\rangle = H(t)|\Psi(t)\rangle \tag{18}$$

can be written in the form

$$|\Psi(t)\rangle = \sum_m a_m(t)e^{-im\omega_0 t}|\psi_m\rangle, \tag{19}$$

where the coefficient a_n obeys the following equation:

$$\frac{\partial a_m}{\partial t} = -\sum_n a_n e^{i(m-n)\omega_0 t}\langle\varphi_m|\frac{\partial}{\partial t}|\psi_n\rangle. \tag{20}$$

Submitting the expression of $|\varphi_m(t)\rangle$ and $|\psi_n(t)\rangle$, we have

$$\frac{\partial a_n}{\partial t} = \frac{1}{\omega_0}\frac{\partial \kappa}{\partial t}(a_{n-1}e^{i\omega_0 t} - a_{n+1}e^{-i\omega_0 t}), \tag{21}$$

which is the starting point for the following discussions.

In this work, we consider the case with $\kappa(t) = \kappa_0\cos(\omega t)$, where κ_0 can be a complex number. Taking the rotating-wave approximation (RWA) under the condition $|\omega - \omega_0| \ll \omega_0$, we have

$$i\frac{\partial a_n}{\partial t} = \frac{\kappa_0\omega}{2\omega_0}[a_{n-1}e^{i(\omega_0-\omega)t} + a_{n+1}e^{i(\omega-\omega_0)t}]. \tag{22}$$

We focus on the dynamics of the system at resonance $\omega = \omega_0$, in which the equation becomes

$$i\frac{\partial a_n}{\partial t} = \frac{\kappa_0}{2}(a_{n-1} + a_{n+1}). \tag{23}$$

The Schrödinger equation is used for a uniform tight-binding chain.

5 Dynamical exponents

As shown above, the resonant dynamics are essentially governed by the simple equivalent Hamiltonian

$$H_{\text{eq}} = \frac{\kappa_0}{2}\sum_{n=-\infty}^{+\infty}(|n\rangle\langle n+1| + \text{H.c}), \tag{24}$$

where $|n\rangle$ denotes the eigenstates of the instantaneous Hamiltonian. The dynamics of H_{eq} were investigated in Ref. [16], which indicates that the reality of κ_0 plays an important role in the dynamics. The Hamiltonian H_{eq} can be diagonalized in the form

$$H_{\text{eq}} = \sum_{k\in(-\pi,\pi)}\varepsilon_k|k\rangle\langle k|, \tag{25}$$

with

$$|k\rangle = \frac{1}{\sqrt{2\pi}}\sum_l e^{ikl}|l\rangle, \tag{26}$$

and the spectrum

$$\varepsilon_k = \kappa_0\cos k. \tag{27}$$

The time evolution of state

$$\begin{aligned} |\Psi(t)\rangle &= \sum_l a_l(t)|l\rangle \\ &= \sum_l a_l(0)\sum_n i^{n-l}J_{n-l}(-\kappa_0 t)|n\rangle, \end{aligned} \tag{28}$$

can be obtained for any given $\{a_l(0)\}$. Intuitively, an initial state $|0\rangle$ (or $a_l(0)=\delta_{0l}$) could spread out and never return whether κ_0 is real or complex. In the following, we focus on two cases with $\kappa_0=1$ and $\kappa_0=i$.

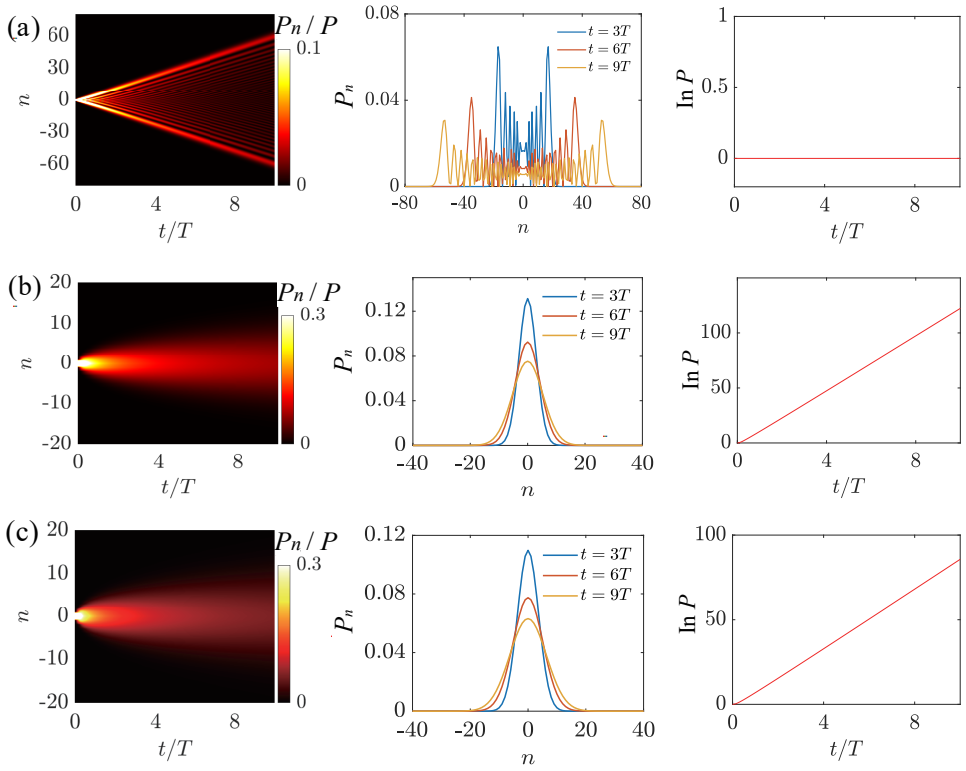

Figure 4: The same plots of $P_n(t)/P(t)$ and $\ln P(t)$ as those in Fig. 2 are shown for several typical values of system parameters but at a resonance $\omega_0=\omega=1$. Here, (a), (b), and (c) correspond to the cases with $\kappa_0=1$, i, and $e^{i\pi/4}$, respectively. The middle panels correspond to the probability distributions at moments $t=3T$, $6T$, and $9T$, respectively. The right panels are the logarithmic plots of total probabilities as functions of time. These results agree with our analytical analysis in the main text. We can see that the patterns in (b) and (c) are almost identical. This inidcates that the imaginary part of hopping plays the important role in the energy-level spreading.

(i) $\kappa_0=1$; in this case, the straightforward derivation yields

$$a_n(t)=i^n J_n(-t), \tag{29}$$

which ensures the probability distribution of the energy levels

$$\mathcal{P}_n(t)=|a_n(t)|^2=|J_n(-t)|^2, \tag{30}$$

and

$$\mathcal{P}=\sum_n \mathcal{P}_n(t)=1. \tag{31}$$

The feature of the Bessel function indicates that there exists a maximum at the edge of $\mathcal{P}_n(t)$, which can be regarded as the wave front of the occupied-energy-level spreading. The location of such a wave front can then be determined by the equation

$$\frac{\partial \mathcal{P}_{n_c}(t)}{\partial t} = 0. \tag{32}$$

Based on the relations of Bessel functions

$$\begin{aligned} J_{n_c-1}(x) - J_{n_c+1}(x) &= 2J'_{n_c}(x) \\ J_{n_c+1}(x) + J_{n_c-1}(x) &= 2\,|n_c/t|\,J_{n_c}(x), \end{aligned} \tag{33}$$

we have

$$2J_{n_c+1}(-t) = 2|n_c/t|J_{n_c}(-t). \tag{34}$$

For large n and t, we have $J_{n_c+1}(-t) \approx J_{n_c}(-t)$, which results in

$$|n_c| \approx t. \tag{35}$$

Then, we conclude that the dynamical exponent of occupied-energy-level spreading is $z = 1$.

(ii) $\kappa_0 = i$; in parallel, the corresponding amplitude is the Bessel function with imaginary argument

$$\begin{aligned} a_{2n}(t) &= (-1)^n J_{2n}(-it) \\ &= \frac{(-1)^n}{2\pi}\int_{-\pi}^{\pi} \cos(2nk) e^{-t\sin k}\mathrm{d}k, \end{aligned} \tag{36}$$

and

$$\begin{aligned} a_{2n+1}(t) &= i(-1)^n J_{2n+1}(-it) \\ &= \frac{(-1)^{n+1}}{2\pi i}\int_{-\pi}^{\pi} \sin[(2n+1)k] e^{-t\sin k}\mathrm{d}k. \end{aligned} \tag{37}$$

On a long time scale, the main contribution to the integral comes from the integrand around $k = -\pi/2$. Then, we have

$$a_{2n}(t) \approx e^{-\frac{(2n)^2}{t}} \frac{1}{2\pi}\int_{-\pi}^{\pi} e^{-t\sin k}\mathrm{d}k, \tag{38}$$

and

$$a_{2n+1}(t) \approx e^{-\frac{(2n+1)^2}{t}} \frac{1}{2\pi i}\int_{-\pi}^{\pi} e^{-t\sin k}\mathrm{d}k, \tag{39}$$

with small ε_k, which results in the probability distribution of the energy levels

$$\mathcal{P}_n(t) = |a_n(t)|^2 \approx \sqrt{\frac{2}{\pi t}}\mathcal{P} e^{-\frac{2n^2}{t}}, \tag{40}$$

with the total probability

$$\mathcal{P} = \sum_n \mathcal{P}_n = \frac{1}{2\pi}\int_{-\pi}^{\pi} e^{-2t\sin k}\mathrm{d}k. \tag{41}$$

Obviously, the profile of $\mathcal{P}_n$ is a Gaussian type, and the total probability grows exponentially as e^{2t} approaches the large t limit. In this situation, the dynamics of occupied-energy-level spreading can be characterized by the full width at half maximum (FWHM),

$$\mathcal{P}_{n_c}(t) = \frac{1}{2}\mathcal{P}_0(t), \tag{42}$$

which results in

$$|n_c| \approx \sqrt{t}. \tag{43}$$

Then, we conclude that the dynamical exponent of occupied-energy-level spreading is $z = 1/2$.

To verify and demonstrate the above analysis, numerical simulations are performed to investigate the dynamic behavior of dynamic processes at resonance with $\omega = \omega_0$. For the same initial state as shown in Fig. 2, the plots of $P_n(t)$ and $P(t)$ for several typical values of κ_0 are presented in Fig. 4. These numerical results agree with our above analysis in two aspects: (i) At resonance, the dynamics are no longer periodic; (ii) The level spreading exhibits distinct behaviors for Hermitian and non-Hermitian systems.

6 2D simulator via wavepacket dynamics

In this section, we will show how the time evolution of a wavepacket in an engineered time-independent 2D square lattice can simulate our results for Floquet dynamics in a 1D time-dependent lattice. In experiments, single-particle hopping dynamics can be simulated by discretized spatial light transport in an engineered 2D square lattice of evanescently coupled optical waveguides [29]. A 2D lattice can be fabricated by coupled waveguides, by which the temporal evolution of the single-particle probability distribution in the 2D lattice can be visualized by the spatial propagation of the light intensity.

We consider a single-particle Hamiltonian on a square lattice

$$\begin{aligned} H_{2D} &= \kappa_0 \sum_{n,m=-\infty}^{\infty} \cos(qm)\,|n,m\rangle\langle n+1,m| - J \sum_{n,m=-\infty}^{\infty} |n,m\rangle\langle n,m+1| + \text{h.c.} \\ &\quad + \omega_0 \sum_{n,m=-\infty}^{\infty} n|n,m\rangle\langle n,m|, \end{aligned} \tag{44}$$

which is an array of coupled 1D Bloch systems with q-dependent hopping strength $\kappa_0 \cos(qm)$. Fig. 1(b) shows a schematic of the system. According to the above analysis, the system is governed by Bloch dynamics with frequency ω_0 for vanishing J, regardless of whether κ_0 is real or complex.

Now, we start to investigate the dynamics in the presence of nonzero J. The k-space representation of the Schrödinger equation

$$i\frac{\partial}{\partial t}|\psi\rangle = H_{2D}|\psi\rangle, \tag{45}$$

can be written as

$$\begin{aligned} i\frac{\partial \psi}{\partial t} &= \kappa_0 \cos k_x [\psi(k_x, k_y + q, t) + \psi(k_x, k_y - q, t)] \\ &\quad + i\omega_0 \frac{\partial \psi}{\partial k_x} - 2J \cos k_y \psi(k_x, k_y, t), \end{aligned} \tag{46}$$

by taking the Fourier transformation

$$|k_x, k_y\rangle = \frac{1}{2\pi} \sum_{n,m=-\infty}^{\infty} e^{i(k_x n + k_y m)}|n,m\rangle. \tag{47}$$

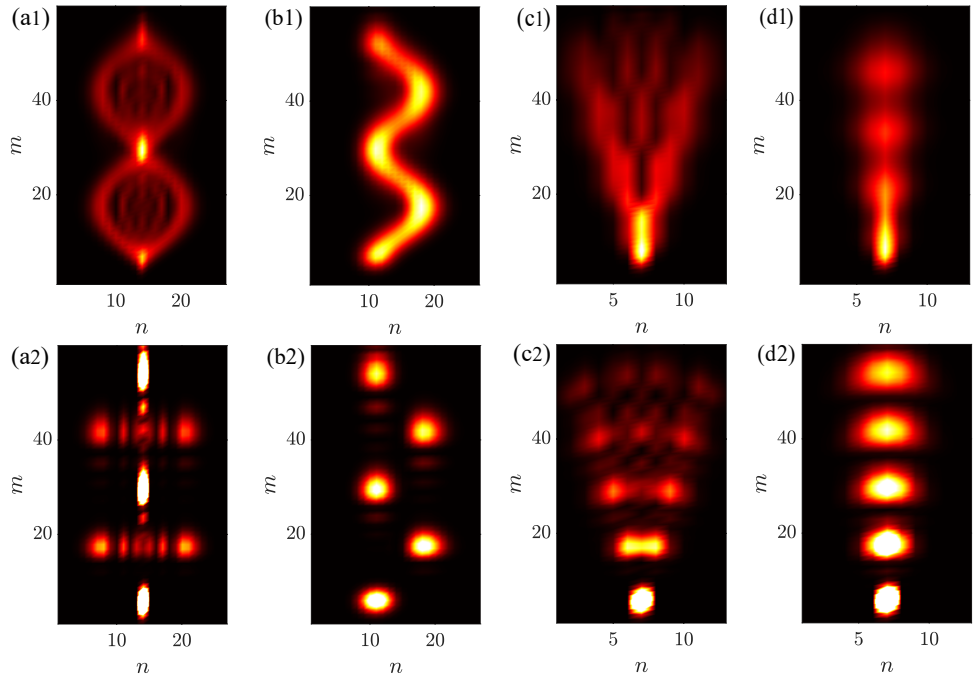

Figure 5: For numerical simulations of the dynamics, the trajectories of wavepackets evolving in the in a 2D lattice with four typical configurations were obtained. The traces of the wavepacket $P(n,m)$ for the time evolutions of the four cases are shown in (a1), (b1), (c1), and (d1). The probability distributions $p(n,m,t)$ for the time evolutions of four representative cases at $t=0$, $t=2\pi/J$, $t=4\pi/J$, $t=6\pi/J$ and $t=8\pi/J$ are shown in (a2), (b2), (c2), and (d2), respectively. The initial states and system parameters are given in the main text. The size of the system is 60×30. The energy scale of the Hamiltonian is taken as $J=1$. The probability distributions on the square lattice exhibit distinct patterns corresponding to the dynamic behaviors of Bloch breathing, oscillation, diffusion and superdiffusion.

For the case with $q=0$, the solution $\psi\left(k_x,k_y,t\right)$ reduces to

$$\psi\left(k_x,k_y,t\right)=f\left(k_x,t\right)e^{it2J\cos k_y}, \tag{48}$$

where $f\left(k_x,t\right)$ obeys the following equation:

$$i\frac{\partial f}{\partial t}=(2\kappa_0\cos k_x+i\omega_0\frac{\partial}{\partial k_x})f\left(k_x,t\right). \tag{49}$$

In the case with $k_y\approx\pi/2$, we have $\cos k_y\approx k_y-\pi/2$. One can construct a solution by the superposition of states $|k_x,k_y\rangle$ with $k_y\approx\pi/2$ in the form [30]

$$\begin{aligned}|g\left(k_x,t\right)\rangle &= (\frac{2\alpha^2}{\pi})^{1/4}\int_{-\pi}^{\pi}e^{-\alpha^2\left(k_y-\pi/2\right)^2}e^{it2J\cos k_y}\times f\left(k_x,t\right)\mathrm{d}k_y|k_x,k_y\rangle\\ &\approx (\frac{1}{2\pi\alpha^2})^{1/4}\sum_m e^{im\pi/2}e^{-(1/4)(m-2Jt)^2/\alpha^2}\times f\left(k_x,t\right)|k_x,m\rangle,\end{aligned} \tag{50}$$

which is a traveling Gaussian wavepacket in the y direction. It is presumed that such a solution still holds true by taking $\kappa_0\to\kappa_0\cos\left(qm\right)$ when $\kappa_0\cos\left(qm\right)$ varies slowly during the extension of the wavepacket in the y direction due to the locality of the solution. In this sense, the traveling wavepacket experiences an adiabatic process, after which the independence of the

Table 1: List of the parameters of the four driven Hamiltonians and initial states, where $y(m)=(4\pi^2)^{-1/4}e^{im\pi/2}e^{-m^2/4}$.

	κ_0	ω	ω_0	Initial state
(i)	J	0	$0.5J$	$y(m)\delta_{n,n_0}$
(ii)	J	0	$0.5J$	$y(m)e^{-n^2/4}$
(iii)	$0.25J$	$0.5J$	$0.5J$	$y(m)\delta_{n,n_0}$
(iv)	$0.25iJ$	$0.5J$	$0.5J$	$y(m)\delta_{n,n_0}$

dynamics in both directions is maintained. Obviously, a small value of q should be needed. On the other hand, the value of ω_0 must match q when the system is employed to simulate the dynamics at the resonance. To this end, a small value of κ_0 should be taken to maintain the Stark ladder.

Actually, under the conditions $\kappa_0 \ll J$ and $k_y \approx \pi/2$, such a 2D system is equivalent to a coupled waveguide array due to the linear dispersion in the y direction, in which the tunneling rate between neighboring waveguides is m dependent. The speed of the propagating wavepacket along m is $2J$. To simulate the dynamics along x, one can simply take $q=\omega/(2J)$, regarding m as the temporal coordinate.

To determine the dynamics of the square lattice system, we perform numerical simulations. We compute the time evolutions for the initial state in the form

$$\psi(n,m,0)=(\frac{1}{4\pi^2\alpha^4})^{1/4}e^{im\pi/2}e^{-(1/4)(m^2+n^2)/\alpha^2}, \tag{51}$$

in the following four representative cases. (i) To simulate Bloch breathing, the initial state is taken as $\psi(0,m,0)\delta_{n,n_0}$ with $\alpha=1$. The system parameters are $\kappa_0=J$, $\omega=0$ and $\omega_0=0.5J$. (ii) To simulate Bloch oscillation, the initial state is taken as $\psi(n,m,0)$ with $\alpha=1$. The system parameters are $\kappa_0=J$, $\omega=0$ and $\omega_0=0.5J$. (iii) To simulate superdiffusion, the initial state is taken as $\psi(0,m,0)\delta_{n,n_0}$ with $\alpha=1$. The system parameters are $\kappa_0=0.25J$ and $\omega=\omega_0=0.5J$. (iv) To simulate diffusion, the initial state is taken as $\psi(0,m,0)\delta_{n,n_0}$ with $\alpha=1$. The system parameters are $\kappa_0=0.25Ji$ and $\omega=\omega_0=0.5J$. For greater clarity, the specific parameters are shown in Tab. 1. The evolved state has the form

$$|\psi(n,m,t)\rangle=e^{-iH_{2D}t}|\psi(n,m,0)\rangle, \tag{52}$$

which can be computed by exact diagonalization.

The probability distribution at position (n,m) at time t is defined by the Dirac probabilities

$$p(n,m,t)=|\langle n,m,|\psi(n,m,t)\rangle|^2. \tag{53}$$

To visualize the profile of the dynamics, we define the function

$$P(n,m)=\sum_{j=1}p(n,m,j\tau), \tag{54}$$

to record the trace of the wavepacket. Here, we use $j\tau$ to denote the discretized time coordinate. It is expected that the distribution of $P(n,m)$ exhibits patterns similar to those in Fig. 4. The numerical results presented in Fig. 5 show that the probability distributions on the square lattice exhibit distinct patterns corresponding to the dynamic behaviors of Bloch breathing, oscillation, diffusion and superdiffusion.

7 Conclusion

In summary, we simultaneously examine the effects of non-Hermiticity and periodic driving on a Stark ladder system. The most fascinating and important feature of such systems is that the Stark ladder can be maintained regardless of the non-Hermiticity of the hopping strength, and the energy level spacing depends only on its norm. This allows us to solve the problem in an analytical manner. The Bloch oscillation is broken when the Floquet frequency is resonant with the energy level spacing, and the occupied energy levels spread out. Furthermore, analytic analysis and numerical simulation show that the level-spreading dynamics for real and complex hopping strengths exhibit distinct behaviors of superdiffusion and diffusion, respectively. In addition, we propose a scheme to simulate the results by wavepacket dynamics in a 2D square lattice. This can be experimentally realized in the coupled array of waveguides. These findings may help us deepen our understanding of the interplay between non-Hermiticity and periodic driving impacts on the dynamics of the system.

Acknowledgements

Funding information This work was supported by the National Natural Science Foundation of China (under Grant No. 12374461).

References

[1] N. Moiseyev, *Non-Hermitian quantum mechanics*, ISBN 978-0-521-88972-8 (2011).

[2] D. J. Tannor, *Introduction to Quantum Mechanics: A time-dependent perspective*, University Science Books, USA, ISBN 13978-1-891389-23-8 (2007).

[3] L. Zhou and J. Gong, *Non-Hermitian Floquet topological phases with arbitrarily many real-quasienergy edge states*, Phys. Rev. B **98**, 205417 (2018), doi:10.1103/PhysRevB.98.205417.

[4] M. S. Rudner and L. S. Levitov, *Topological Transition in a Non-Hermitian Quantum Walk*, Phys. Rev. Lett. **102**, 065703 (2009), doi:10.1103/PhysRevLett.102.065703.

[5] R. J. León-Montiel, M. A. Quiroz-Juárez, J. L. Domínguez-Juárez, R. Quintero-Torres, J. L. Aragón, A. K. Harter and Y. N. Joglekar, *Observation of slowly decaying eigenmodes without exceptional points in Floquet dissipative synthetic circuits*, Commun. Phys. **1**(1) (2018), doi:10.1038/s42005-018-0087-3.

[6] J. Li, A. K. Harter, J. Liu, L. de Melo, Y. N. Joglekar and L. Luo, *Observation of parity-time symmetry breaking transitions in a dissipative Floquet system of ultracold atoms*, Nat. Commun. **10**(1) (2019), doi:10.1038/s41467-019-08596-1.

[7] P. He and Z. H. Huang, *Floquet engineering and simulating exceptional rings with a quantum spin system*, Phys. Rev. A **102**, 062201 (2020), doi:10.1103/PhysRevA.102.062201.

[8] E. N. Blose, *Floquet topological phase in a generalized $\mathcal{PT}$-symmetric lattice*, Phys. Rev. B **102**(10), 104303 (2020), doi:10.1103/physrevb.102.104303.

[9] L. Zhou, *Non-Hermitian Floquet topological superconductors with multiple Majorana edge modes*, Phys. Rev. B **101**(1), 014306 (2020), doi:10.1103/physrevb.101.014306.

[10] X. Zhang and J. Gong, *Non-Hermitian Floquet topological phases: Exceptional points, coalescent edge modes, and the skin effect*, Phys. Rev. B **101**(4), 045415 (2020), doi:10.1103/physrevb.101.045415.

[11] L. Xiao, T. Deng, K. Wang, G. Zhu, Z. Wang, W. Yi and P. Xue, *Non-Hermitian bulkboundary correspondence in quantum dynamics*, Nat. Phys. **16**(7), 761 (2020), doi:10.1038/s41567-020-0836-6.

[12] D. S. Ageev, A. A. Bagrov and A. A. Iliasov, *Deterministic chaos and fractal entropy scaling in Floquet conformal field theories*, Phys. Rev. B **103**(10), l100302 (2021), doi:10.1103/physrevb.103.l100302.

[13] M. Glück, *WannierStark resonances in optical and semiconductor superlattices*, Phys. Rep. **366**(3), 103 (2002), doi:10.1016/s0370-1573(02)00142-4.

[14] S. Longhi, *Bloch oscillations in non-Hermitian lattices with trajectories in the complex plane*, Phys. Rev. A **92**(4), 042116 (2015), doi:10.1103/physreva.92.042116.

[15] E. M. Graefe, H. J. Korsch and A. Rush, *Quasiclassical analysis of Bloch oscillations in non-Hermitian tight-binding lattices*, New J. Phys. **18**(7), 075009 (2016), doi:10.1088/1367-2630/18/7/075009.

[16] S. Longhi, *Non-Hermitian bidirectional robust transport*, Phys. Rev. B **95**(1), 014201 (2017), doi:10.1103/physrevb.95.014201.

[17] C. Qin, B. Wang, Z. J. Wong, S. Longhi and P. Lu, *Discrete diffraction and Bloch oscillations in non-Hermitian frequency lattices induced by complex photonic gauge fields*, Phys. Rev. B **101**(6), 064303 (2020), doi:10.1103/physrevb.101.064303.

[18] K. Zhan, X. Kang, L. Dou, T. Zhao, Q. Chen, Q. Zhang, G. Han and B. Liu, *Rectified Bloch oscillations in dynamically modulated waveguide arrays*, Opt. Express **30**(25), 45110 (2022), doi:10.1364/oe.475734.

[19] H. Zhao, *Identifying Diffusion Processes in One-Dimensional Lattices in Thermal Equilibrium*, Phys. Rev. Lett. **96**(14), 140602 (2006), doi:10.1103/physrevlett.96.140602.

[20] R. Metzler, E. Barkai and J. Klafter, *Anomalous diffusion and relaxation close to thermal equilibrium: A fractional Fokker-Planck equation approach*, Phys. Rev. Lett. **82**(18), 3563 (1999), doi:10.1103/PhysRevLett.82.3563.

[21] J. P. Bouchaud and A. Georges, *Anomalous diffusion in disordered media: Statistical mechanisms, models and physical applications*, Phys. Rep. **195**(45), 127 (1990), doi:10.1016/0370-1573(90)90099-n.

[22] T. Hartmann, F. Keck, H. J. Korsch and S. Mossmann, *Dynamics of Bloch oscillations*, New J. Phys. **6**, 2 (2004), doi:10.1088/1367-2630/6/1/002.

[23] F. Bloch, *Elektron im periodischen Potential, Bändermodell des Festkörpers, Z*, Phys **52**, 555 (1928).

[24] Proc. R. soc. Lond. Ser. A-Contain. Pap. Math. Phys. Character. **145**(855), 523 (1934), doi:10.1098/rspa.1934.0116.

[25] C. Waschke, H. G. Roskos, R. Schwedler, K. Leo, H. Kurz and K. Köhler, *Coherent submillimeter-wave emission from Bloch oscillations in a semiconductor superlattice*, Phys. Rev. Lett. **70**(21), 3319 (1993), doi:10.1103/physrevlett.70.3319.

[26] M. Ben Dahan, E. Peik, J. Reichel, Y. Castin and C. Salomon, *Bloch Oscillations of Atoms in an Optical Potential*, Phys. Rev. Lett. **76**(24), 4508 (1996), doi:10.1103/physrevlett.76.4508.

[27] S. R. Wilkinson, C. F. Bharucha, K. W. Madison, Q. Niu and M. G. Raizen, *Observation of Atomic Wannier-Stark Ladders in an Accelerating Optical Potential*, Phys. Rev. Lett. **76**(24), 4512 (1996), doi:10.1103/physrevlett.76.4512.

[28] B. P. Anderson and M. A. Kasevich, *Macroscopic Quantum Interference from Atomic Tunnel Arrays*, Science **282**(5394), 1686 (1998), doi:10.1126/science.282.5394.1686.

[29] D. N. Christodoulides, F. Lederer and Y. Silberberg, *Discretizing light behaviour in linear and nonlinear waveguide lattices*, Nature **424**(6950), 817 (2003), doi:10.1038/nature01936.

[30] W. Kim, L. Covaci and F. Marsiglio, *Impurity scattering of wave packets on a lattice*, Phys. Rev. B **74**(20), 205120 (2006), doi:10.1103/physrevb.74.205120.